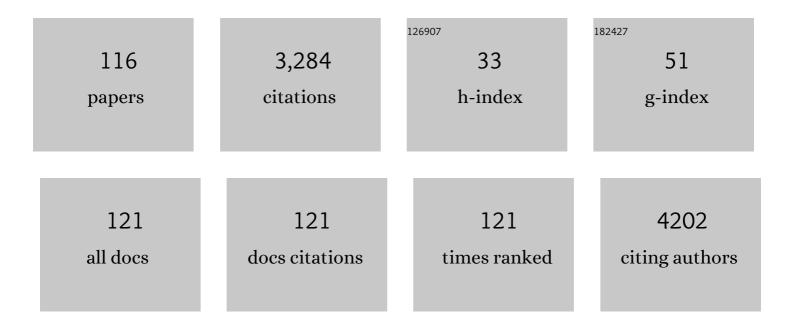
## Michel Koole

List of Publications by Year in descending order

Source: https://exaly.com/author-pdf/412812/publications.pdf Version: 2024-02-01



#	Article	IF	CITATIONS
1	Phase 1 Study of the Pittsburgh Compound B Derivative <sup>18</sup> F-Flutemetamol in Healthy Volunteers and Patients with Probable Alzheimer Disease. Journal of Nuclear Medicine, 2009, 50, 1251-1259.	5.0	273
2	Whole-Body Biodistribution and Radiation Dosimetry of <sup>18</sup> F-GE067: A Radioligand for In Vivo Brain Amyloid Imaging. Journal of Nuclear Medicine, 2009, 50, 818-822.	5.0	200
3	Bone scintigraphy with <sup>99m</sup> technetium-hydroxymethylene diphosphonate allows early diagnosis of cardiac involvement in patients with transthyretin-derived systemic amyloidosis. Amyloid: the International Journal of Experimental and Clinical Investigation: the Official Journal of the International Society of Amyloidosis. 2014. 21. 35-44.	3.0	129
4	99mTc-ECD brain perfusion SPET: variability, asymmetry and effects of age and gender in healthy adults. European Journal of Nuclear Medicine and Molecular Imaging, 2001, 28, 873-887.	2.1	108
5	Increased Expression of Translocator Protein (TSPO) Marks Pro-inflammatory Microglia but Does Not Predict Neurodegeneration. Molecular Imaging and Biology, 2018, 20, 94-102.	2.6	88
6	Preclinical Evaluation of a P2X7 Receptor–Selective Radiotracer: PET Studies in a Rat Model with Local Overexpression of the Human P2X7 Receptor and in Nonhuman Primates. Journal of Nuclear Medicine, 2016, 57, 1436-1441.	5.0	77
7	Calibration of gamma camera systems for a multicentre European 123I-FP-CIT SPECT normal database. European Journal of Nuclear Medicine and Molecular Imaging, 2011, 38, 1529-1540.	6.4	73
8	Preclinical Evaluation of <sup>18</sup> F-JNJ64349311, a Novel PET Tracer for Tau Imaging. Journal of Nuclear Medicine, 2017, 58, 975-981.	5.0	72
9	Quantifying SV2A density and drug occupancy in the human brain using [11C]UCB-J PET imaging and subcortical white matter as reference tissue. European Journal of Nuclear Medicine and Molecular Imaging, 2019, 46, 396-406.	6.4	72
10	Preclinical Evaluation of <sup>18</sup> F-JNJ41510417 as a Radioligand for PET Imaging of Phosphodiesterase-10A in the Brain. Journal of Nuclear Medicine, 2010, 51, 1584-1591.	5.0	64
11	Whole-Body Biodistribution and Radiation Dosimetry of the Cannabinoid Type 2 Receptor Ligand [11C]-NE40 in Healthy Subjects. Molecular Imaging and Biology, 2013, 15, 384-390.	2.6	64
12	<sup>18</sup> F-JNJ-64413739, a Novel PET Ligand for the P2X7 Ion Channel: Radiation Dosimetry, Kinetic Modeling, Test-Retest Variability, and Occupancy of the P2X7 Antagonist JNJ-54175446. Journal of Nuclear Medicine, 2019, 60, 683-690.	5.0	63
13	[18F]AlF-NOTA-octreotide PET imaging: biodistribution, dosimetry and first comparison with [68Ga]Ga-DOTATATE in neuroendocrine tumour patients. European Journal of Nuclear Medicine and Molecular Imaging, 2020, 47, 3033-3046.	6.4	59
14	In vivo synaptic density loss is related to tau deposition in amnestic mild cognitive impairment. Neurology, 2020, 95, e545-e553.	1.1	56
15	[11C]JNJ54173717, a novel P2X7 receptor radioligand as marker for neuroinflammation: human biodistribution, dosimetry, brain kinetic modelling and quantification of brain P2X7 receptors in patients with Parkinson's disease and healthy volunteers. European Journal of Nuclear Medicine and Molecular Imaging, 2019, 46, 2051-2064.	6.4	55
16	A Standardized Method for the Construction of Tracer Specific PET and SPECT Rat Brain Templates: Validation and Implementation of a Toolbox. PLoS ONE, 2015, 10, e0122363.	2.5	52
17	Loss of Presynaptic Terminal Integrity in the Substantia Nigra in Early Parkinson's Disease. Movement Disorders, 2020, 35, 1977-1986.	3.9	52
18	Positron Emission Tomography (PET) Quantification of GABAA Receptors in the Brain of Fragile X Patients. PLoS ONE, 2015, 10, e0131486.	2.5	52

#	Article	IF	CITATIONS
19	Optimized In Vivo Detection of Dopamine Release Using <sup>18</sup> F-Fallypride PET. Journal of Nuclear Medicine, 2012, 53, 1565-1572.	5.0	49
20	Proposal for the standardisation of multi-centre trials in nuclear medicine imaging: prerequisites for a European 123I-FP-CIT SPECT database. European Journal of Nuclear Medicine and Molecular Imaging, 2012, 39, 188-197.	6.4	48
21	[123I]FP-CIT ENC-DAT normal database: the impact of the reconstruction and quantification methods. EJNMMI Physics, 2017, 4, 8.	2.7	46
22	Use of Multimodal Imaging and Clinical Biomarkers in Presymptomatic Carriers of <i>C9orf72</i> Repeat Expansion. JAMA Neurology, 2020, 77, 1008.	9.0	45
23	<sup>68</sup> Ga-NOTA-Functionalized Ubiquicidin: Cytotoxicity, Biodistribution, Radiation Dosimetry, and First-in-Human PET/CT Imaging of Infections. Journal of Nuclear Medicine, 2018, 59, 334-339.	5.0	44
24	Quantification of <sup>18</sup> F-JNJ-42259152, a Novel Phosphodiesterase 10A PET Tracer: Kinetic Modeling and Test–Retest Study in Human Brain. Journal of Nuclear Medicine, 2013, 54, 1285-1293.	5.0	43
25	TSPO Versus P2X7 as a Target for Neuroinflammation: An In Vitro and In Vivo Study. Journal of Nuclear Medicine, 2020, 61, 604-607.	5.0	42
26	Transient changes in the endocannabinoid system after acute and chronic ethanol exposure and abstinence in the rat: a combined PET and microdialysis study. European Journal of Nuclear Medicine and Molecular Imaging, 2013, 40, 1582-1594.	6.4	41
27	Experimental Performance Assessment of SPM for SPECT Neuroactivation Studies Using a Subresolution Sandwich Phantom Design. NeuroImage, 2002, 16, 200-216.	4.2	40
28	Whole-Body Biodistribution and Radiation Dosimetry of the Human Cannabinoid Type-1 Receptor Ligand <sup>18</sup> F-MK-9470 in Healthy Subjects. Journal of Nuclear Medicine, 2008, 49, 439-445.	5.0	38
29	Micro-Positron Emission Tomography Imaging of Rat Brain Metabolism during Expression of Contextual Conditioning. Journal of Neuroscience, 2012, 32, 254-263.	3.6	38
30	Pretargeted PET Imaging Using a Bioorthogonal <sup>18</sup> F-Labeled <i>trans</i> -Cyclooctene in an Ovarian Carcinoma Model. Bioconjugate Chemistry, 2017, 28, 2915-2920.	3.6	38
31	Regional Accuracy of ZTE-Based Attenuation Correction in Static [18F]FDG and Dynamic [18F]PE2I Brain PET/MR. Frontiers in Physics, 2019, 7, .	2.1	38
32	Micro-flow photosynthesis of new dienophiles for inverse-electron-demand Diels–Alder reactions. Potential applications for pretargeted in vivo PET imaging. Chemical Science, 2017, 8, 1251-1258.	7.4	37
33	Human biodistribution and dosimetry of 18F-JNJ42259152, a radioligand for phosphodiesterase 10A imaging. European Journal of Nuclear Medicine and Molecular Imaging, 2013, 40, 254-261.	6.4	36
34	Transfer of normal 99mTc-ECD brain SPET databases between different gamma cameras. European Journal of Nuclear Medicine and Molecular Imaging, 2001, 28, 435-449.	2.1	33
35	Feasibility of [18F]-RGD for ex vivo imaging of atherosclerosis in detection of αvβ3 integrin expression. Journal of Nuclear Cardiology, 2015, 22, 1179-1186.	2.1	32
36	What We Observe In Vivo Is Not Always What We See In Vitro: Development and Validation of 11C-JNJ-42491293, A Novel Radioligand for mGluR2. Journal of Nuclear Medicine, 2017, 58, 110-116.	5.0	31

#	Article	lF	CITATIONS
37	Synaptic density in healthy human aging is not influenced by age or sex: a 11C-UCB-J PET study. NeuroImage, 2021, 232, 117877.	4.2	31
38	Non-uniform versus uniform attenuation correction in brain perfusion SPET of healthy volunteers. European Journal of Nuclear Medicine and Molecular Imaging, 2001, 28, 90-98.	2.1	30
39	Al18F-NOTA-octreotide: first comparison with 68Ga-DOTATATE in a neuroendocrine tumour patient. European Journal of Nuclear Medicine and Molecular Imaging, 2019, 46, 2398-2399.	6.4	30
40	Validation of Parametric Methods for [11C]UCB-J PET Imaging Using Subcortical White Matter as Reference Tissue. Molecular Imaging and Biology, 2020, 22, 444-452.	2.6	28
41	Inflammation-Based Index and <sup>68</sup> Ga-DOTATOC PET–Derived Uptake and Volumetric Parameters Predict Outcome in Neuroendocrine Tumor Patients Treated with <sup>90</sup> Y-DOTATOC. Journal of Nuclear Medicine, 2020, 61, 1014-1020.	5.0	28
42	Preclinical evaluation of [ <sup>18</sup> F]MA3: a CB <sub>2</sub> receptor agonist radiotracer for PET. British Journal of Pharmacology, 2019, 176, 1481-1491.	5.4	26
43	Translation of HDAC6 PET Imaging Using [ <sup>18</sup> F]EKZ-001–cGMP Production and Measurement of HDAC6 Target Occupancy in Nonhuman Primates. ACS Chemical Neuroscience, 2020, 11, 1093-1101.	3.5	26
44	Synaptic Damage and Its Clinical Correlates in People With Early Huntington Disease. Neurology, 2022, 98, .	1.1	26
45	Non-invasive methods for absolute cerebral blood flow measurement using 99mTc-ECD: a study in healthy volunteers. European Journal of Nuclear Medicine and Molecular Imaging, 2001, 28, 862-872.	2.1	25
46	Quantification and discriminative power of 18F-FE-PE2I PET in patients with Parkinson's disease. European Journal of Nuclear Medicine and Molecular Imaging, 2020, 47, 1913-1926.	6.4	24
47	11C-MK-8278 PET as a Tool for Pharmacodynamic Brain Occupancy of Histamine 3 Receptor Inverse Agonists. Journal of Nuclear Medicine, 2014, 55, 65-72.	5.0	23
48	Quantification of TSPO overexpression in a rat model of local neuroinflammation induced by intracerebral injection of LPS by the use of [18F]DPA-714 PET. European Journal of Nuclear Medicine and Molecular Imaging, 2016, 43, 163-172.	6.4	23
49	Synthesis and preclinical evaluation of [ 11 C]MA-PB-1 for inÂvivo imaging of brain monoacylglycerol lipase (MAGL). European Journal of Medicinal Chemistry, 2017, 136, 104-113.	5.5	23
50	Moving Toward Multicenter Therapeutic Trials in Amyotrophic Lateral Sclerosis: Feasibility of Data Pooling Using Different Translocator Protein PET Radioligands. Journal of Nuclear Medicine, 2020, 61, 1621-1627.	5.0	22
51	Preclinical Evaluation and Quantification of <sup>18</sup> F-FPEB as a Radioligand for PET Imaging of the Metabotropic Glutamate Receptor 5. Journal of Nuclear Medicine, 2015, 56, 1954-1959.	5.0	21
52	Preclinical Safety Evaluation and Human Dosimetry of [18F]MK-6240, a Novel PET Tracer for Imaging Neurofibrillary Tangles. Molecular Imaging and Biology, 2020, 22, 173-180.	2.6	21
53	In vivo synaptic density relates to glucose metabolism at rest in healthy subjects, but is strongly modulated by regional differences. Journal of Cerebral Blood Flow and Metabolism, 2021, 41, 0271678X2098150.	4.3	21
54	InÂvivo evidence for long-term vascular remodeling resulting from chronic cerebral hypoperfusion in mice. Journal of Cerebral Blood Flow and Metabolism, 2017, 37, 726-739.	4.3	20

#	Article	IF	CITATIONS
55	Kinetic modeling and longâ€term testâ€retest reproducibility of the mGluR5 PET tracer <sup>18</sup> Fâ€FPEB in human brain. Synapse, 2016, 70, 153-162.	1.2	18
56	Preclinical Evaluation and Quantification of 18F-Fluoroethyl and 18F-Fluoropropyl Analogs of SCH442416 as Radioligands for PET Imaging of the Adenosine A2A Receptor in Rat Brain. Journal of Nuclear Medicine, 2017, 58, 466-472.	5.0	18
57	Characterization of the novel GlyT1 PET tracer [ <sup>18</sup> F]MKâ€6577 in humans. Synapse, 2015, 69, 33-40.	1.2	17
58	Endothelial Msx1 transduces hemodynamic changes into an arteriogenic remodeling response. Journal of Cell Biology, 2015, 210, 1239-1256.	5.2	17
59	Positron emission tomography imaging of cerebral glucose metabolism and type 1 cannabinoid receptor availability during temporal lobe epileptogenesis in the amygdala kindling model in rhesus monkeys. Epilepsia, 2018, 59, 959-970.	5.1	17
60	Local pulmonary drug delivery in the preterm rabbit: feasibility and efficacy of daily intratracheal injections. American Journal of Physiology - Lung Cellular and Molecular Physiology, 2019, 316, L589-L597.	2.9	17
61	Single-word comprehension deficits in the nonfluent variant of primary progressive aphasia. Alzheimer's Research and Therapy, 2018, 10, 68.	6.2	16
62	Distinct [18F]THK5351 binding patterns in primary progressive aphasia variants. European Journal of Nuclear Medicine and Molecular Imaging, 2018, 45, 2342-2357.	6.4	16
63	Clinical validation of the novel HDAC6 radiotracer [18F]EKZ-001 in the human brain. European Journal of Nuclear Medicine and Molecular Imaging, 2021, 48, 596-611.	6.4	16
64	Construction and Evaluation of Quantitative Small-Animal PET Probabilistic Atlases for [18F]FDG and [18F]FECT Functional Mapping of the Mouse Brain. PLoS ONE, 2013, 8, e65286.	2.5	16
65	Synthesis and biological evaluation of carbon-11 and fluorine-18 labeled tracers for in vivo visualization of PDE10A. Nuclear Medicine and Biology, 2014, 41, 695-704.	0.6	15
66	Combined brain and spinal FDG PET allows differentiation between ALS and ALS mimics. European Journal of Nuclear Medicine and Molecular Imaging, 2020, 47, 2681-2690.	6.4	15
67	Cross-Modal Distillation to Improve MRI-Based Brain Tumor Segmentation With Missing MRI Sequences. IEEE Transactions on Biomedical Engineering, 2022, 69, 2153-2164.	4.2	15
68	Spatial decrease of synaptic density in amnestic mild cognitive impairment follows the tau build-up pattern. Molecular Psychiatry, 2022, 27, 4244-4251.	7.9	15
69	[18F] <scp>JNJ</scp> 42259152 binding to phosphodiesterase 10A, a key regulator of medium spiny neuron excitability, is altered in the presence of cyclic <scp>AMP</scp> . Journal of Neurochemistry, 2016, 139, 897-906.	3.9	14
70	Evaluation of androgen-induced effects on the uptake of [18F]FDG, [11C]choline and [11C]acetate in an androgen-sensitive and androgen-independent prostate cancer xenograft model. EJNMMI Research, 2013, 3, 31.	2.5	13
71	Striatal phosphodiesterase 10A availability is altered secondary to chronic changes in dopamine neurotransmission. EJNMMI Radiopharmacy and Chemistry, 2017, 1, 3.	3.9	13
72	Lower regional gray matter volume in the absence of higher cortical amyloid burden in late-life depression. Scientific Reports, 2021, 11, 15981.	3.3	13

#	Article	IF	CITATIONS
73	Changes in synaptic density in the subacute phase after ischemic stroke: A 11C-UCB-J PET/MR study. Journal of Cerebral Blood Flow and Metabolism, 2021, , 0271678X2110477.	4.3	12
74	Biodistribution and radiation dosimetry of radioiodinated hypericin as a cancer therapeutic. International Journal of Oncology, 2014, 44, 819-829.	3.3	11
75	Total Body Metabolic Tumor Response in ALK Positive Non-Small Cell Lung Cancer Patients Treated with ALK Inhibition. PLoS ONE, 2016, 11, e0149955.	2.5	11
76	Prospective comparison of simultaneous [68Ga]Ga-PSMA-11 PET/MR versus PET/CT in patients with biochemically recurrent prostate cancer. European Radiology, 2022, 32, 901-911.	4.5	11
77	Three-dimensional rotational angiography fused with multimodal imaging modalities for targeted endomyocardial injections in the ischaemic heart. European Heart Journal Cardiovascular Imaging, 2014, 15, 900-907.	1.2	10
78	Regional glucose metabolic decreases with ageing are associated with microstructural white matter changes: a simultaneous PET/MR study. European Journal of Nuclear Medicine and Molecular Imaging, 2022, 49, 664-680.	6.4	10
79	The PET tracer [ <sup>11</sup> C]MK-6884 quantifies M4 muscarinic receptor in rhesus monkeys and patients with Alzheimer's disease. Science Translational Medicine, 2022, 14, eabg3684.	12.4	10
80	Impact of meningeal uptake and partial volume correction techniques on [ <sup>18</sup> F]MK-6240 binding in aMCI patients and healthy controls. Journal of Cerebral Blood Flow and Metabolism, 2022, 42, 1236-1246.	4.3	10
81	Brain PET imaging of phosphodiesterase 10A in progressive supranuclear palsy and Parkinson's disease. Movement Disorders, 2017, 32, 943-945.	3.9	9
82	A dual-time-window protocol to reduce acquisition time of dynamic tau PET imaging using [18F]MK-6240. EJNMMI Research, 2021, 11, 49.	2.5	9
83	The geometric transfer function for a slat collimator mounted on a strip detector. IEEE Transactions on Nuclear Science, 2005, 52, 708-713.	2.0	8
84	Convolutional Neural Networks for Brain Tumor Segmentation Using Different Sets of MRI Sequences. , 2019, , .		8
85	Pharmacokinetic modeling of [11C]flumazenil kinetics in the rat brain. EJNMMI Research, 2017, 7, 17.	2.5	7
86	Glucose metabolic brain patterns to discriminate amyotrophic lateral sclerosis from Parkinson plus syndromes. EJNMMI Research, 2018, 8, 110.	2.5	7
87	Monte Carlo Simulations of the GE Signa PET/MR for Different Radioisotopes. Frontiers in Physiology, 2020, 11, 525575.	2.8	7
88	Targeted alpha therapy: a critical review of translational dosimetry research with emphasis on actinium-225. Quarterly Journal of Nuclear Medicine and Molecular Imaging, 2020, 64, 265-277.	0.7	7
89	Imaging of cardiac and renal perfusion in a rat model with 13N–NH3 micro-PET. International Journal of Cardiovascular Imaging, 2015, 31, 213-219.	1.5	6
90	Minimally invasive quantification of cerebral P2X7R occupancy using dynamic [18F]JNJ-64413739 PET and MRA-driven image derived input function. Scientific Reports, 2021, 11, 16172.	3.3	6

#	Article	IF	CITATIONS
91	Cognitive Decline Assessment: A Review From Medical Imaging Perspective. Frontiers in Aging Neuroscience, 2021, 13, 704661.	3.4	6
92	Parametric Imaging of [11C]Flumazenil Binding in the Rat Brain. Molecular Imaging and Biology, 2018, 20, 114-123.	2.6	5
93	Identifying a glucose metabolic brain pattern in an adeno-associated viral vector based rat model for Parkinson's disease using 18F-FDG PET imaging. Scientific Reports, 2019, 9, 12368.	3.3	5
94	Study of the quantification of FBP SPECT images with a correction for partial volume effects. IEEE Transactions on Nuclear Science, 2002, 49, 69-73.	2.0	4
95	Asymmetric Amyloid Deposition in the Brain Following Unilateral Electroconvulsive Therapy. Biological Psychiatry, 2017, 81, e11-e13.	1.3	4
96	Volume-of-interest-based supervised cluster analysis for pseudo-reference region selection in [18F]DPA-714 PET imaging of the rat brain. EJNMMI Research, 2018, 8, 112.	2.5	4
97	Synthetic Pept-Ins as a Generic Amyloid-Like Aggregation-Based Platform for In Vivo PET Imaging of Intracellular Targets. Bioconjugate Chemistry, 2021, 32, 2052-2064.	3.6	4
98	Preclinical Evaluation of [ <sup>11</sup> C]YC-72-AB85 for <i>In Vivo</i> Visualization of Heat Shock Protein 90 in Brain and Cancer with Positron Emission Tomography. ACS Chemical Neuroscience, 2021, 12, 3915-3927.	3.5	4
99	Influence of detector thickness on resolution in three-headed gamma camera PET. IEEE Transactions on Nuclear Science, 2002, 49, 98-103.	2.0	3
100	Fluoro-D-glucose-micro positron emission tomography as a diagnostic tool to confirm brain death in a murine donor lung injury model. Journal of Surgical Research, 2013, 180, 343-348.	1.6	3
101	Dual time point method for the quantification of irreversible tracer kinetics: A reference tissue approach applied to [18F]-FDOPA brain PET. Journal of Cerebral Blood Flow and Metabolism, 2017, 37, 3124-3134.	4.3	3
102	ICâ€Pâ€150: [Câ€11]MKâ€6884 PET: CHARACTERIZING BRAIN M4 RECEPTORS IN HEALTHY ELDERLY VOLUNTEE ACETYLCHOLINESTERASE INHIBITORSâ€TREATED AD PATIENTS. Alzheimer's and Dementia, 2019, 15, P121.	RS AND	3
103	Quantitative Whole-Body Diffusion-weighted MRI after One Treatment Cycle for Aggressive Non-Hodgkin Lymphoma Is an Independent Prognostic Factor of Outcome. Radiology Imaging Cancer, 2021, 3, e200061.	1.6	3
104	Human biodistribution and dosimetry of [11C]-UCB-J, a PET radiotracer for imaging synaptic density. EJNMMI Physics, 2021, 8, 37.	2.7	3
105	Abstract OT2-1-10: RAD1901, a novel tissue-selective estrogen receptor degrader (SERD) demonstrates estrogen receptor engagement in a phase 1 clinical study. , 2015, , .		3
106	Twelve-Week Yoga vs. Aerobic Cycling Initiation in Sedentary Healthy Subjects: A Behavioral and Multiparametric Interventional PET/MR Study. Frontiers in Psychiatry, 2021, 12, 739356.	2.6	3
107	Transmission imaging with a moving point source: influence of crystal thickness and collimator type. IEEE Transactions on Nuclear Science, 2005, 52, 166-173.	2.0	2
108	Dual time-point imaging for post-dose binding potential estimation applied to a [ <sup>11</sup> C]raclopride PET dose occupancy study. Journal of Cerebral Blood Flow and Metabolism, 2017, 37, 866-876.	4.3	2

#	Article	IF	CITATIONS
109	The Effect of Aging on Brain Glucose Metabolic Connectivity Revealed by [18F]FDG PET-MR and Individual Brain Networks. Frontiers in Aging Neuroscience, 2021, 13, 798410.	3.4	2
110	Cannabinoid receptor availability modulates the magnitude of dopamine release in vivo in the human reward system: A preliminary multitracer positron emission tomography study. Addiction Biology, 2022, 27, e13167.	2.6	2
111	[18F]JNJ41510417 a potential PET radioligand for imaging phosphodiesterase-10A in the brain. NeuroImage, 2010, 52, S15.	4.2	Ο
112	Low-dose CT-derived attenuation scan: One acquisition, more applications?. Journal of Nuclear Cardiology, 2015, 22, 429-430.	2.1	0
113	An approach for a reconstruction-derived whole-blood arterial input function (RDIF) in PET/MRI. , 2018, , .		Ο
114	Regional distribution of amyloid deposition and grey matter atrophy in lateâ€ <b>i</b> ife depression. Alzheimer's and Dementia, 2020, 16, e041564.	0.8	0
115	PET Quantification in Neuropsychiatry. , 2014, , 15-44.		0
116	Glucose metabolism changes in cerebellar tonsils as an early predictor of cognitive decline. Alzheimer's and Dementia, 2021, 17, .	0.8	0